In vivo analysis of *Staphylococcus aureus* infected mice reveals differential temporal and spatial expression patterns of *fhuD2*

Marta Bacconi[a], Andreas F. Haag[a*], Emiliano Chiarot[a], Paolo Donato[a], Fabio Bagnoli[a], Isabel Delany[a#] and Giuliano Bensi[a#]

GSK Vaccines Srl, Via Fiorentina 1, 53100 Siena, Italy[a]

Running Head: In vivo expression of *S. aureus fhuD2*

[#]Address correspondence to Giuliano Bensi, giuliano.x.bensi@gsk.com and Isabel Delany, isabel.x.delany@gsk.com

*Present address: Institute of Infection, Immunity and Inflammation, College of Medical, Veterinary and Life Sciences, University of Glasgow, 120 University Place, Glasgow, G12 8TA, UK

M.B. and A.F.H. contributed equally to this work and are listed in alphabetical order

ABSTRACT

Staphylococcus aureus is an opportunistic human pathogen and a major cause of invasive infections such as bacteremia, endocarditis, pneumonia and wound infections. FhuD2 is a staphylococcal lipoprotein involved in the uptake of iron-hydroxymate and is under the control of the iron uptake regulator Fur. The protein is part of an investigational multi-component vaccine formulation that has shown protective efficacy in several murine models of infection. Even though *fhuD2* expression was shown to be upregulated in murine kidneys infected with *S. aureus*, it is unknown whether the bacterium undergoes increased iron deprivation during prolonged infection. Furthermore, different infection niches of *S. aureus* might provide different environments and iron availability resulting in different *fhuD2* expression pattern within different host organs. To address these questions, we characterized the *in vitro* expression of the *fhuD2* gene and confirmed Fur-dependent iron-regulation of its expression. We further investigated its expression in mice infected with a bioluminescent reporter strain of *S. aureus* expressing the luciferase operon under the control of the *fhuD2* promoter. The emission of bioluminescence in different organs was followed over a seven-day time course, as well as quantitative real-time PCR analysis of the RNA transcribed from the endogenous *fhuD2* gene. Using this approach, we could show that *fhuD2* expression was induced during infection in all organs analyzed and that differences in expression were observed in the temporal expression profiles, and between infected organs. Our data suggest that *S. aureus* undergoes increased iron deprivation during progression of infection in diverse host organs and accordingly induces dedicated iron acquisition mechanisms. Since FhuD2 plays a central role in providing the pathogen with the required iron, further knowledge of the patterns of *fhuD2* expression *in vivo* during infection is instrumental in better defining the role of this antigen in *S. aureus* pathogenesis and as a vaccine antigen.

INTRODUCTION

Staphylococcus aureus is a Gram-positive pathogen commonly isolated within the hospital environment (1). *S. aureus* is part of the normal flora of the skin and nares and it is estimated that up to 30% of the human population are long-term asymptomatic carriers of the bacterium (2). *S. aureus* can cause a wide range of disease manifestations ranging from suppurative and subcutaneous skin infections to severe and systemic infections such as pneumonia, sepsis, septic arthritis, endocarditis and osteomyelitis (3, 4). Infections can become persistent as the bacterium disseminates throughout the host causing abscess formation (5). Progression to disease is often opportunistic and affects both immunocompromised and immunocompetent patients. *S. aureus* was the cause of over 80,000 severe MRSA infections resulting in more than 11,000 deaths in 2011 in the US alone reaching a death toll comparable to that of HIV (6).

The capacity of *S. aureus* to cause a wide spectrum of human disease reflects its ability to adapt to distinct microenvironments in the human body. The pathogenesis of *S. aureus* infection is a complex process involving a tight regulation of numerous virulence factors. *S. aureus* presents heterogeneity through variability in gene and protein expression in response to environmental factors (7).

Iron is of key importance for the metabolism of *S. aureus* as it acts as a cofactor for numerous proteins involved in central metabolism and respiration. Upon encountering iron limiting conditions, *S. aureus* up-regulates dedicated iron uptake systems as well as glycolysis and down-regulates the tricarboxylic acid (TCA) cycle. Under extreme iron limitation the electron transfer chain is inactivated and the bacterium survives under fermentative growth (8). The TCA cycle involves numerous enzymes that require iron as a cofactor (9). Glycolysis generates ATP independently of respiration resulting in the accumulation of pyruvate and

lactate. Lactate was shown to be secreted by iron-starved *S. aureus*, resulting in acidification of the surrounding medium. It was suggested that this acidification might contribute to the liberation of iron from the host sequestration proteins transferrin and lactoferrin (8).

Iron availability is severely limited during infection and the ability of *S. aureus* to sequester iron from the host significantly influences its pathogenesis. Expression of iron-regulated genes is under the control of the ferric iron uptake regulator Fur. In *S. aureus* Fur also indirectly contributes to coordinated repression of secreted hemolysins and cytotoxins. Under iron limiting conditions, Fur repression is relieved and up-regulation of these factors occurs. On the other hand, Fur contributes positively to the expression of immunomodulatory proteins, including superantigens, protein A, complement inhibitory protein SCIN, and chemotaxis inhibitor CHIP (10). A Fur inactivated mutant was shown to be less virulent in a murine pneumonia model of infection as it was unable to respond adequately to innate immunity (10), suggesting that in the absence of this key regulatory protein, *i.e.* in a strain that constitutively expresses an iron starvation response, virulence is compromised. Under iron limitation, *S. aureus* induces the expression of a number of siderophores, siderophore and xenosiderophore transport systems, as well as heme-related iron sequestration mechanisms (11, 12). *S. aureus* has evolved a dedicated transport system for the uptake of xenosiderophores of the ferric-hydroxymate type consisting of an ATP-binding cassette transporter encoded by the *fhuCBG* operon and two lipoprotein receptors FhuD1 and FhuD2 (13, 14). In *S. aureus* FhuD1 and FhuD2 paralogues possess different specificities for various hydroxamate siderophores tested (15, 16) and FhuD2 appears to bind exclusively to hydroxamate xenosiderophores, *e.g*. ferrichrome, coprogen and aerobactin (17, 18). FhuD2 expression was shown to be induced via reporter gene fusions in the absence of iron or Fur(18, 19), respectively.

FhuD2 is part of a vaccine formulation that has been shown to be protective in different mouse models of infection (15, 16, 20). It has been shown to contribute to bacterial survival in mouse bacteremia and kidney abscess models (16). Furthermore, gene expression appeared to be up-regulated approximately 8-fold in bacteria isolated from host kidneys four days after infection (16), suggesting that the presence of FhuD2 was important for establishing infection and dissemination of the bacteria already at an early stage. In addition to kidneys, *S. aureus* is also known to disseminate into heart, lung and liver tissues as well as into joints and bones upon intravenous infection in animal models. Previous studies have focused solely on a single time-point or individual organs when characterizing the expression of *fhuD2*. However, we lack information as to the extent of iron deprivation *S. aureus* undergoes when localizing in different host organs and throughout the course of its infection. To fill this gap in our understanding of *S. aureus* pathogenesis, here, we characterized the temporal and spatial expression profiles of *fhuD2* within the aforementioned mouse organs throughout the infection process. Interestingly, we found that expression of *fhuD2* increased at later stages of *S. aureus* infection and that expression levels between organs differed.

RESULTS

The *fhuD2* gene and its regulatory motifs are conserved in all available *S. aureus* strains

FhuD1 and FhuD2 are two lipoproteins involved in binding iron (III)-hydroxymates (18). The genes encoding these lipoproteins are located in different genomic loci (Fig. 1A) and are distant from each other and from the genes encoding the transmembrane proteins of the *fhu* ABC transporter. To evaluate the conservation of the *fhuD* genes across circulating *S. aureus* isolates, we assessed the presence of the respective gene in 4135 available genome sequences. BLAST analysis showed that *fhuD1* was present only in 35.3% (1461/4135) of the staphylococcal genomes while *fhuD2* was conserved in all genomes analyzed. Both *fhuD1* and *fhuD2* genes showed high identity across different strains (>97%) but showed significantly lower identities when compared with each other (approximately 42% amino acid identity and 65% amino acid similarity). These results suggest that while FhuD1 is dispensable and only in a subset of *S. aureus* strains analyzed, FhuD2 is present and highly conserved in all strains, and is likely the main player involved in iron-hydroxymate acquisition.

In order to address whether regulatory elements within the *fhuD2* promoter were conserved among *S. aureus* isolates, we aligned the 213 bp intergenic sequence between *fhuD2* and the upstream gene (NWMN_2186, an acyl-CoA dehydrogenase-related protein) of 4135 *S. aureus* isolates and calculated a phylogenetic distance tree (Fig. 1B). The intergenic region of the *fhuD2* gene showed more than 99% identity and clustered into eight clades, defined by segregating SNPs which were neither present in the predicted promoter nor in regulatory regions within the promoter sequence (Fig. 1C). Expression of *fhuD2* is proposed to be regulated by the ferric uptake repressor Fur and consistent with this a completely conserved Fur recognition sequence was identified immediately upstream of the ribosomal binding site of

fhuD2 (Fig. 1C). This analysis therefore suggested that the regulation of *fhuD2* expression is conserved among various staphylococcal strains.

Fur controls *fhuD2* promoter in an iron availability dependent manner

With the purpose of evaluating the *fhuD2* promoter activity *in vitro* and *in vivo* we used a reporter plasmid, pMABA-Par/TA-P_{fhuD2}-*lux*, with the *lux*-operon of *Photorhabdus luminescens* under the control of the 213 bp-long upstream region of the gene containing the *fhuD2* promoter from the *S. aureus* Newman strain. The plasmid, had been molecularly engineered to be stably maintained *in vitro* and *in vivo* in the absence of a selective antibiotic pressure (21).

To investigate iron and Fur mediated regulation of *fhuD2 in vitro*, we constructed a *fur* deletion mutant in the Newman strain, transformed both the wild type and the *fur* mutant strains with the pMABA-Par/TA-P_{fhuD2}-*lux* plasmid, and compared bioluminescence emission during *in vitro* growth of these strains in the presence or absence of iron over a time course experiment. The Fur mutant was slightly impaired in its growth in complex media, and while it grew identically to the wild type strain during early and mid-exponential growth, it only reached a final OD_{600} of 6, while the wild type strain reached a OD_{600} of more than 12 (data not shown) similarly to what has been previously reported (19).

Newman wild type and *fur* mutant strains harboring either pMABA-Par/TA-P_{fhuD2}-lux or the pMABA-Par/TA-lux promoterless control were grown to early-exponential phase (OD_{600} 0.5-0.7) and iron was removed by the addition of dipyridyl to a final concentration of 1 mM. Samples for bioluminescence determination as well as for mRNA extraction were taken immediately prior to dipyridyl addition and after 30 and 60 min of incubation. The bioluminescent signal was normalized to the number of CFU ml^{-1} present at the time of

measurement. Bioluminescence was induced 4-fold in the wild-type strain on chelation of iron (Fig 2A) while constitutively high levels of bioluminescence were measured in the Fur mutant irrespective of the condition (Fig 2B). The expression levels of *fhuD2* mRNA from the endogenous gene were assessed by qRT-PCR and they increased between 7 to 10-fold following addition of dipyridyl in the wild-type (Fig 2C). Conversely, *fhuD2* mRNA levels in the Δ*fur* mutant were approximately 5- to 8-fold higher than in the wild type strain in all conditions (Fig. 2D). These data indicate that Fur represses transcription of *fhuD2* in the presence of iron. In addition, bioluminescence resulting from *fhuD2* promoter activity on the episomal reporter showed a pattern similar to that of the mRNA levels in each strain from the endogenous gene. The kinetics of induction were slightly faster and the overall increase was slightly higher for mRNA levels with respect to bioluminescence, however, the regulation of the reporter system and of the endogenous *fhuD2* gene *in vitro* were aligned, confirming that the *fhuD2*/luciferase system was a faithful reporter system in vitro.

fhuD2 is spatially and temporally regulated during _in vivo_ infection progression

To assess temporal and spatial regulation of *fhuD2 in vivo*, we infected CD1 mice intravenously with 10^7 CFU of exponentially growing *S. aureus* strain Newman carrying either the pMABA-Par/TA-P_{fhuD2}-lux reporter or the promoterless control plasmids. The initial inoculum was prepared from cultures at OD 2.0, a growth phase corresponding to maximal *fhuD2* mRNA expression under *in vitro* culturing (Fig. S1). In order to follow *fhuD2* promoter expression *in vivo* in real time and to visualize spatially where the *fhuD2* promoter was most active, we measured the emitted bioluminescence at two, four and seven days post-infection by means of an IVIS Spectrum-CT® imaging system. A time-dependent increase of the signals was observed (Fig. 3). No bioluminescence was observed in mice infected with the Newman

179 strain transformed with the promoterless control plasmid (data not shown). When mice were
180 infected with Newman *fhuD2* reporter strain (carrying pMABA-Par/TA-P_{fhuD2}-*lux),* we observed
181 bioluminescent signals in diverse locations in all animals tested suggesting that bacterial
182 infection and/or the expression of the reporter *lux* gene were disseminated over the course of
183 time (Fig 3A), furthermore the overall bioluminescence increased over time (3B). In addition,
184 3D-computer tomography (CT) analysis was performed to localize the origin of the
185 bioluminescent signals in mice more precisely (Fig. 4). Clear bioluminescent signals
186 manifested at the posterior leg joints already two days after the infection (Fig. 3A) and 3D
187 reconstruction and CT section analyses confirmed that bacteria had also infected the knee
188 joint and the femoral bone tissue (Fig. 4 B, D, and F). Four and seven days after infection,
189 bioluminescence was detected in kidneys (Fig. 3A). Interestingly, CT analysis confirmed that
190 bioluminescence could be superimposed in some cases onto darker patches observed in
191 kidneys, likely corresponding to abscesses (Fig. 4B, C and E). This would be consistent with
192 the fact that bacteria are present together with a large number of neutrophils (22) and *fhuD2*
193 is expressed in these structures where bacteria accumulate. Finally, later during the infection,
194 bioluminescence was observed in the abdominal area corresponding to the liver and heart, as
195 evidenced by 3D and CT section analyses (Fig. 4H and I). In addition, bioluminescence
196 persisted in joints and increased in kidneys (Fig. 3A), suggesting that either the bacterial
197 burden or *fhuD2* expression had increased over time.
198 To determine whether the higher signal intensities in diverse organs and during infection
199 progression were related to higher bacterial burden, increased *fhuD2* expression or both,
200 heart, lungs, liver and kidneys were collected from infected mice at two, four and seven days
201 after infection, and CFU/organ, bioluminescence and endogenous *fhuD2*-specific mRNA were
202 measured *ex vivo*. Joint washes were not included in this analysis since the very low amount

of total cellular/bacterial RNA obtained from the samples did not allow us to obtain a consistent RNA quantification necessary to perform the quantitative real-time PCR at all the time points.

The determination of CFU numbers demonstrated differential progression of the infection in the different niches (Fig. 5). Bacteria quickly spread into the various organs and bacterial burdens averaging between 10^4 and 10^6 CFU of organ homogenate were measured two days after infection. Heart and kidneys exhibited the highest bacterial load per organ with approximately 10^6 CFU. While lung and liver both exhibited a bacterial load averaging between 10^4 and 10^5. The lungs of the mice remained with the lowest burden with only a slight increase in bacterial load ($<10^6$ per lung) at 7 days. An approximately 2 log increase in CFU/organ was observed in liver, heart and kidney organs 7 days after infection. Kidneys consistently exhibited the highest bacterial load in all mice with $>10^8$CFU.

We calculated the relative bioluminescent signal per bacterial cell in the different organs for each time point and we normalized expression levels to the relative bioluminescent signal per bacterial cell of the inoculum prior to infection. Expressing the data as fold increase in bioluminescence relative to the inoculum over time (temporally) for each organ (Fig. 6, A-D) and for each time point among the different organs (spatially) (Fig. S2), allowed us to obtain an informative picture of *fhuD2* expression in the course of the infection. The specific activity of the *fhuD2* promoter was higher in all organs compared to the inoculum. While we could not observe bioluminescence *in vivo* with the IVIS analysis in the lung, bioluminescence was measured *ex vivo* in lung homogenates reached over 12-fold increases even at the earliest time point after infection (2 days) and was maintained throughout the observation period (Fig. 6B). Bioluminescence in kidneys and liver instead was lower (approximately 2-fold) at the initial stages of infection and augmented with time to a maximum of 16- and 32-fold increases

respectively at 4 days post infection with respect to the initial inoculum (Fig. 6C and D). Instead approximately 6-fold increase in bioluminescence was observed in the heart at day two post-infection which increased to over 20-fold at the last time point (Fig. 6A).

We extracted RNA from infected organs at the defined time points and performed quantitative real-time PCR to measure the *fhuD2* mRNA levels of the chromosomal *fhuD2* gene during the course of infection. Expression data were normalized to the mRNA levels of *fhuD2* in the inoculum used to infect mice. Overall, expression of the endogenous *fhuD2* gene mRNA, although not mirroring identically, followed a similar pattern to that observed for the bioluminescent reporter construct (Fig. 6 E-H and S2 D-F) showing levels 14-fold compared to the inoculum at all timepoints in the lung, increasing from <10-fold at 2 days to >10-fold during the course of the infection in the liver and kidneys, and a less evident increase which did not reach more than 10-fold in the heart. In general, variability of mRNA expression was lower when compared to variability observed with the bioluminescent reporter construct and induction kinetics appeared to be faster.

DISCUSSION

Iron sequestration is an important antimicrobial mechanism exerted by the infected host, which attempts to limit iron availability to concentrations far below those permitting bacterial growth (23). Nevertheless, bacteria have developed sophisticated strategies to circumvent iron limitation during host infection (24, 25), including high affinity iron scavenging mechanisms. FhuD2, an iron-scavenging lipoprotein, has been shown to play a role in the early dissemination of *S. aureus* during infection in animal models (16). Furthermore, immunization of mice with the FhuD2 recombinant protein consistently confers protection from *S. aureus* challenge in diverse models of infection and against a broad range of staphylococcal isolates (16, 20). Here, we characterize the factors regulating the expression of this candidate vaccine antigen *in vitro* and we evaluated the temporal and spatial expression pattern of *fhuD2* in mice infected with *S. aureus*.

The *S. aureus* strain used for this study was Newman. This choice was based not only on its known robust performance in various infection models (26), but also because the main regulatory motifs in the intergenic region upstream of *fhuD2* were conserved in over 4000 strains analyzed, suggesting that regulation of expression of this gene would also be conserved among different isolates. Evaluation of a *fhuD2* reporter construct under *in vitro* conditions confirmed that *fhuD2* expression was controlled by Fur in an iron-dependent manner and that the episomal reporter closely reproduced the transcription pattern of the endogenous *fhuD2* gene. We observed a slight temporal delay between the profile of mRNA steady state levels and the bioluminescent measurement of the reporter where maximal bioluminescence occurs later than maximal mRNA levels. This is most likely due to transcriptional and translational delay of the reporter expression. Maximal expression levels of

fhuD2 were observed in the absence of Fur or iron indicating that Fur acts as a repressor to *fhuD2* when it is bound to Fe^{2+}.

Signals from the bioluminescent reporter allowed the monitoring of *fhuD2* promoter activity *in vivo* after infection but were influenced by the depth of the host organ from the animal's body surface, and possibly other factors. We therefore evaluated temporal and spatial expression profiles of the *S. aureus fhuD2* gene by combining *in vivo* imaging in live mice, with *ex vivo* measurements of specific bioluminescence in the organ homogenates in relation to bacterial load as well as the direct quantification of target gene mRNA as a further control.

The 2D and 3D in vivo imaging of bioluminescence from the reporter strain permitted us to perform a qualitative evaluation of the exact localization, at the organ and tissue level, of bacteria expressing the reporter gene *in vivo*. Bioluminescent signals could be assigned early after the infection not only at joints but also in the femur in clear areas of infected bone. This observation was consistent with the known tropism of *S. aureus* for joints and bones causing arthritis and osteomyelitis (27). Signals at joints were either steady or increased during infection progression, suggesting active bacterial replication and/or higher expression levels of *fhuD2* in this environment. As quantitative RT-PCR could not be performed on infected joint and bone samples due to the presence of relatively few bacteria, tracking expression by bioluminescent reporter was the only informative approach on gene expression in this niche. While bacterial load is low, early bioluminescence signals were more easily detected in limbs likely due to their peripheral location and to the presence of bacteria in a liquid environment. Similarly, 2D and 3D IVIS analyses allowed the observation of intense signals detected in kidneys, in which we could associate *fhuD2*-driven bioluminescence spots and denser areas, likely representing abscesses. This observation is consistent with reports indicating that *S. aureus* finds an iron deficient environment within murine kidney abscesses (28), which

could trigger induction of *fhuD2* gene expression. Interestingly, we frequently noticed that in some animals one of the two kidneys would not be visible after a certain time during the 3D reconstruction, and we hypothesize that in these cases the kidney functionality may be compromised to such an extent that the contrast agent would no longer be able to penetrate the organ. Finally, the IVIS analysis also allowed confirmation of the induced luciferase reporter activity in liver tissue while bioluminescence in hearts was only observed once, and we were unable to detect any bioluminescence in lungs. The difficulty in observing bioluminescence in these organs, in spite of the detectable CFUs and of *fhuD2* promoter activity detected and quantified by bioluminescence/RNA measured in the homogenized organs, may be dependent on multiple factors, such as overall low bacterial burden, promoter activation rate, availability of ATP and oxygen necessary for the bioluminescent reaction, and depth of the emitting signal but more likely to the lack of accumulation in abscesses.

A different approach was instead necessary to perform quantitative measurements of *fhuD2* promoter activation *in vivo*. This was accomplished by collecting the different organs and determining the specific bioluminescence per CFU, as well as the *fhuD2*-specific mRNA content per CFU, to quantify the *fhuD2* promoter activity in the different organs over time and confirm that the reporter and mRNA content patterns were aligned. Expression of *fhuD2* promoter was considerably increased in all in vivo samples with respect to that of the initial inoculum, and interestingly maximal induction levels measured (>10-fold) were significantly higher than the maximal *in vitro* levels either under iron-limiting conditions or in the absence of the Fur repressor, indicating that level of activation of *fhuD2* gene expression in the host environment cannot be reached under *in vitro* conditions.

Furthermore, this analysis highlighted that the *fhuD2* promoter is differentially regulated in diverse organs during time. Bioluminescence at day 2 post infection was higher in lungs (>12-

312 fold) as compared to the other organs analyzed, and was maintained fairly steadily during
313 infection progression, suggesting that *fhuD2* promoter induction is triggered early during
314 infection of the lung. This is in agreement with recent studies demonstrating that *S. aureus*
315 binds considerable amounts of hemoglobin in airways tracts, suggesting that the lung is an
316 iron-poor environment like the heart (29, 30), which would favor *fhuD2* gene activation. In fact,
317 excess of iron in lungs can contribute to the formation of reactive oxygen species which can
318 damage lung tissue and iron is therefore complexed by ferritin and transferrin to prevent this
319 reaction (31-33).
320 Interestingly, expression levels appeared lower at 2 days post infection in other organs such
321 as heart, liver and kidneys and generally increased not only with increasing bacterial burden
322 in the diverse host organs but also with the duration of the infection until reaching a maximum
323 fold-induction of 10 to 20. Overall, activation of the bioluminescent reporter appeared to
324 correlate well with the transcription of the endogenous gene, although some differences could
325 be observed at days four and seven post infection. The observed trend for gradual *fhuD2*
326 induction in hearts, livers and kidneys, more evident in BLI than in mRNA analysis, could
327 suggest that *S. aureus* does not immediately necessitate the acquisition of iron *via* the Fhu
328 system in all organs and that iron availability within different host organs in general becomes
329 more limiting with progression of the infection. In particular, the highest expression was
330 observed in the kidney in areas likely to correspond to abscesses, reported to be sites of
331 calprotectin accumulation and severe cation limitation (34). The liver is considered to be one
332 of the major iron storage sites within vertebrates (35, 36) and an increased initial availability of
333 iron in this organ could explain delayed induction of *S. aureus fhuD2*.
334 *S. aureus* has evolved a dedicated iron uptake system that shows high specificity for human
335 hemoglobin mediated through the hemoglobin receptor IsdB (37). Humanized mice

expressing human hemoglobin were found to be more susceptible to systemic staphylococcal infections highlighting *S. aureus* adaptation to its host (37). In contrast, the FhuD system is involved in scavenging xenosiderophores present in the host environment (13, 15, 18, 38, 39). Xenosiderophores are iron scavenging molecules that are can be present in the environment and are produced by other organisms than *S. aureus*. The ability of *S. aureus* to use these xenosiderophores as an iron source provides the bacterium with a fitness advantage as it is itself not burdened with their biosynthesis (38). A functioning xenosiderophore uptake system contributes to staphylococcal survival and dissemination within the murine host (16) indicating the presence and utilization of these or similar molecules during infection. The stimulus controlling *fhuD2* expression is mediated through Fur and dependent on the available quantities of iron in the environment (12). As such, expression levels of *fhuD2* should accurately reflect the conditions in which *S. aureus* was monitored. To date, the majority of infection studies with *S. aureus* have been performed using wild-type mice and humanized mice have mainly focused on immune factors (37). As non-humanized mice were used in our studies, we cannot fully rule out that the reduced ability of *S. aureus* to use murine hemoglobin might influence expression levels of *fhuD2* to some extent. Increased virulence of *S. aureus* in mice expressing human hemoglobin (37) suggest that *S. aureus* might be able to tap into hemoglobin as alternative iron source in some of the organs analyzed. However, the ability of *S. aureus* to recover iron from host hemoglobin was also shown to be non-essential for staphylococcal infection and resulted only in a slight increase of bacterial burden in mouse livers expressing human hemoglobin compared to wild-type mice (37).

S. aureus employs a multitude of virulence factors in order to establish successful colonization and infection. However, to date, expression studies of virulence factors during staphylococcal infection have focused only on single time points and/or a limited number of

360 virulence-related genes. Others have focused on changes between colonization states rather
361 than progression within specific host organs. For example, adhesion factors such as *clfA*, *clfB*
362 and *sdrC* were shown to be induced during nasal colonization of a cotton rat model(40), while
363 they appeared to be downregulated during bacteremia (40). Conversely, among other
364 adhesins, *clfA*, *sdrC* and *fnbA* were expressed more actively in bacteria colonizing murine
365 hearts (40). However, comparison of expression data in this study is somewhat complicated
366 by the fact the different animal models were compared to each other (cotton rat and mouse).
367 The role and induction of SdrC in nasal colonization was recently corroborated in a deep
368 sequencing study of RNA expression levels of human volunteers colonized with *S. aureus*
369 (41). This study further identified that the expression of genes involved in host-immune
370 evasion such as the staphylococcal complement inhibitor (*scn*), the chemotaxis inhibitor (*chp*)
371 as well as the expression of the secreted toxins such as hemolysins and leukocidins was
372 induced (41). A study investigating gene expression of *S. aureus* during acute and chronic
373 osteomyelitis in a murine model (42) also confirmed the expression of adhesion, immune
374 evasion and nutrient acquisition mechanisms during prolonged infection. In particular during
375 the chronic phase of osteomyelitis, *S. aureus* was shown to gear its gene expression towards
376 products involved in the stringent response, host tissue degradation and nutrient acquisition
377 (42). Consistent with our data, *S. aureus* undergoes increased nutrient and iron deprivation
378 during prolonged infection.
379 Monitoring the expression levels of bacterial genes during host infection is challenging and
380 different methods for analyzing *in vivo* gene expression have advantages and disadvantages.
381 Measuring RNA or protein levels *in vivo* is laborious and can be hampered by low bacterial
382 RNA concentration as we found with the limb and joint analyses in this study or by the
383 complexity of the host tissues not permitting precise protein or RNA quantification. In this

study, the use of a stable episomal reporter plasmid, and a combination of *in vivo* imaging and *ex vivo* quantification of bioluminescence gave accurate and informative information about *fhuD2* expression. Furthermore, the widespread activation of *fhuD2* highlights that the use of iron-regulated promoter reporters for tracking bacterial dissemination in *in vivo* models is an interesting approach.

The data that we have here reported demonstrate that *fhuD2* is expressed *in vivo* in multiple organs and that its expression is spatially and temporally regulated increasing at later infection stages in some organs. This knowledge further supports the inclusion of FhuD2 in the recently proposed vaccine formulation (20), since the induction of an effective FhuD2-mediated immune response could result in protection against *S. aureus* at different stages of infection.

MATERIALS AND METHODS

Bacterial strains and culture conditions. *S. aureus* strains used in this study are defined in Table 1. Strains were grown at 37°C in Tryptic soy broth (TSB, Difco Laboratories) or in trypticase soy agar (TSA) supplemented with 10 µg ml^{-1} of chloramphenicol and 5% (v/v) of sheep blood if required. For the preparation of bacterial challenge inoculum for infection studies in animals, an aliquot of bacteria (2 ml) frozen in PBS (Phosphate-buffered saline) + BSA 10% (w/v) + glutamate 10% (w/v) was thawed, inoculated in 48 ml of TSB (starting from and optical density at 600 nm (OD_{600}) of 0.05) in flasks and incubated at 37°C at 250 rpm until the OD_{600} reached 2. Bacteria were washed twice in equal volumes of PBS, collected by centrifugation for 10 min at 4000 rpm and suspended to 10^8 CFU ml^{-1} to reach the necessary concentration for infection (10^7 CFU per infectious dose).

Sequence analysis

Upstream intergenic sequences of the *fhuD2* gene including 27 nt of the coding sequence were extracted from 4135 *S. aureus* genomes from NCBI databases using BLAST. Sequences were aligned and a phylogenetic tree calculated using Mega 6 (43). The tree was then visualized using the EMBL tree of life tool (44) and clusters identified. Representative strains were selected from each cluster and their intergenic region aligned using CLUSTALW.

Generation of a *fur* deletion mutant. For the generation of a clean *fur* deletion, homologous fragments of approximately 800 nucleotides upstream and downstream of *fur* (NWMN_1406) were amplified using primers NWMN_1406_-796_*Xba*I_F, NWMN_1406_+6_*BamH*I_R, NWMN_1406_+409_*BamH*I_F and NWMN_1406_+1197_*Kpn*I_R. Amplification products were fused by PCR, digested with *Kpn*I and *Sac*I and cloned into pBluescript II SK (+)

creating pBSK-NWMN_1406_del_b. The fused fragment was then amplified from pBSK-NWMN_1406_del_b using primers NWMN_1406_-796_pIMAY_F and NWMN_1406_+1197_pIMAY_R, digested with *Kpn*I and *Sac*I and cloned into pIMAY (45). The plasmid was passed through strain RN4220 and then transformed into strain Newman. Mutant generation was performed as described previously and deletion was verified by PCR using primers NWMN_1406_-837_F and NWMN_1406_+1228_R and sequencing.

Kinetics of *in vitro fhuD2*-promoter driven bioluminescence expression. *S. aureus* strains carrying either the control plasmid pMABA-Par/TA-*lux* (containing the lux operon but lacking the *fhuD2* promoter) or plasmid pMABA-Par/TA-P_{fhuD2}-*lux* (containing the lux operon under the control of the *fhuD2* promoter) were grown overnight in TSB supplemented with 10 µg ml^{-1} of chloramphenicol. One ml of overnight culture was washed once in TSB with chloramphenicol and diluted to a starting OD_{600} of 0.05. Three aliquots of 200 µl per well per strain and tested condition were pipetted into the wells of a black, flat-bottom 96-well plate and the plate incubated at 37°C and 183 rpm in a TECAN Infinite M200pro plate reader. Bioluminescence intensity and absorbance were recorded throughout the whole experiment. Where indicated, dipyridyl was added to induce iron dependent promoter expression once bacteria reached exponential phase growth (OD_{600}≈0.2-0.3 in Tecan).

Induction of *fhuD2* expression by iron chelation. *S. aureus* strains carrying either the control plasmid pMABA-Par/TA-*lux* (containing the lux operon but lacking the *fhuD2* promoter) or plasmid pMABA-Par/TA-P_{fhuD2}-*lux* (containing the lux operon under the control of the *fhuD2* promoter) were grown overnight in TSB supplemented with 10 µg ml^{-1} of chloramphenicol. The following day, 50 ml TSB cultures were inoculated to a starting OD_{600} of 0.05 and grown

445 to exponential phase (0.4-0.7) at 37°C and 250 rpm. At this point iron was either chelated out
446 of the medium by the addition of dipyridyl to a final concentration of 1 mM or the
447 corresponding volume of ethanol (the solvent of dipyridyl) was added to the control culture.
448 Samples for absorbance, bioluminescence and CFU determination as well as for RNA
449 extraction were taken at defined time points.
450
451 **CFU determination.** 20 µl of *S. aureus* culture or organ homogenate were diluted directly in
452 180 µl of ice cold PBS and then 10-fold serially diluted. 10 µl spots of each dilution were
453 transferred onto TSA plates, dried and incubated overnight at 37°C followed by CFU
454 determination.
455
456 **Mouse infections.** Eight to ten-weeks old female CD1 mice (pathogen free) were infected
457 intravenously with a sub-lethal dose of *S. aureus* (~ 1×10^7 CFU per mouse). To assess the
458 promoter activity *in vivo*, heart, lung, liver and kidneys were collected for bioluminescence
459 detection. Each single organ was first homogenized in 2 to 4 ml PBS, and a 100 µl aliquot per
460 single tissue were transferred into a well of a 96 well black plate (Nunc-U96 PP-05ml BLACK)
461 and detected at the IVIS100®. Non-infected mice organs served as control for
462 bioluminescence background. Colony-forming units (CFUs) were determined for each mouse
463 organ.
464
465 ***In vivo* imaging analysis.** 2D *in vivo* imaging acquisition was performed using an IVIS100®
466 instrument. After infection with bioluminescent *S. aureus* strains, mice were anesthetized with
467 a mixture of oxygen and isofluorane (2.5%) and then transferred to the imaging chamber.
468 Bioluminescent images are represented using a pseudo-color scale (blue representing the

469 least-intense and red representing the most-intense light) that was overlaid on a grey-scale
470 image to generate a two-dimensional (2D) picture of the distribution of bioluminescent
471 bacteria in the animal. The acquired image data were saved as 2D arrays containing values
472 corresponding to the number of photons contained within each pixel. For 3D *in vivo* imaging
473 acquisition, an IVIS® Spectrum-CT was utilized. For CT analysis and following 3D
474 reconstruction animals were treated with contrast agents for soft tissues. In particular, we
475 used OptiPrep Density Gradient (SIGMA D1556) to highlight urinary tract organs and Exitron
476 nano 12000 (Miltenyi Biotec) to evidence heart and livers. In both cases, the agents were
477 administered to the mouse by intravenous injection at a concentration of 400 mg kg^{-1} and
478 1800 mg kg^{-1}, respectively. The contrast agents were administered 20 to 30 min before image
479 acquisition. Image data were analyzed using Living Image 4.4 (Xenogen Corporation).
480
481 **Ethics statement.** Mice were monitored twice per day in order to evaluate the early signs of
482 pain and distress according to humane endpoint defined for each model. Animals showing
483 such conditions were euthanized in accordance with experimental protocols, which were
484 reviewed and approved by the local Animal Welfare Body and by the Italian Ministry of Health
485 (protocol number 136/2010-B) for mouse studies.
486
487 **Sample collection, determination of bioluminescence in organ homogenates, RNA**
488 **extraction and cDNA synthesis.** Mouse organs were harvested and homogenized as
489 described above. 100 µl of this homogenate were transferred to a microtiter plate and the
490 bioluminescent signal determined using an IVIS100® instrument. The bioluminescent signal
491 acquired was then related to the CFU/organ of organ homogenate to calculate
492 bioluminescence per bacterium as measurement of promoter activity.

493 For samples for RNA extraction the organs were collected in gentleMACS M tubes (Milteny
494 Biotech) containing 2 to 4 ml of RNAprotect Bacteria Reagent (QIAGEN, Germany) and
495 immediately homogenized. Larger cell debris was removed from the homogenized samples
496 by centrifugation at 100 x g for 5 min and bacteria were thereafter collected by centrifugation
497 for 10 min at 3200 x g. Bacterial pellets were then either directly processed for RNA extraction
498 or stored at -80°C. For RNA extraction, the bacterial pellet was resuspended in 1 ml of Trizol
499 reagent (Ambion) and lysed in a FastPrep®-24 homogenizer (MP Biomedicals) using three
500 cycles of 60 s at 6.5 m s^{-2} followed by 5 min incubation on ice after each cycle. RNA was
501 extracted from the suspension using the Direct-zol™ RNA MiniPrep Kit (Zymo Research)
502 applying an on-column DNase digestion step using the RNase-free DNase kit (QIAgen)
503 according to the manufacturer's instructions. Residual DNA was removed by a second DNase
504 treatment using RQ1 DNase (Promega) followed by RNA purification using the PureLink kit
505 (Ambion) according to the manufacturer's instructions. RNA quality was assessed by gel
506 electrophoresis and Agilent 2100 Bioanalyzer and absence of contaminating DNA confirmed
507 by q-PCR. cDNA was synthetized using the SuperScript First-Strand Synthesis System for
508 RT-PCR (Invitrogen-Life Technologies) according to the manufacturer's instructions, using
509 random hexamer primers for reverse transcription (RT) on 300 to 4000 ng of total RNA.
510
511 **qRT-PCR.** qRT-PCR for *in vivo* mRNA quantification was performed using Platinum SYBR
512 Green qPCR SuperMix-UDG (Invitrogen-Life Technologies) using ROX as internal control on
513 a STRATAGEN Mx3000P QPCR system using the following cycling parameters: 95°C for
514 10 min; 45 cycles of 95°C for 30 s, 55°C for 30 s and 72°C for 30 s; 95°C for 1 min, 55°C for
515 30 s and finally 95°C for 30 s. Final data were analyzed using Genex applying inter-plate

calibration using a control sample. Samples were normalized to the expression levels of *gyrB* and relative expression values to the inoculum were calculated.

Statistical analysis. At least two independent experiments, run under the same conditions, were performed for all studies. Statistical analysis was performed using Graph Pad Prism 6. Expression data were reported as logarithm to generate a Gaussian distribution and outliers determined using the ROUT method (Q=1%). Statistical significance was determined by ANOVA followed Tukey's post-test.

524 **ACKNOWLEDGEMENTS**

525 We would like to thank Olaf Schneewind for the pOS1 plasmid. This work was sponsored by
526 Novartis Vaccines and Diagnostics Srl, now acquired by the GSK group of companies. MB
527 was a recipient of a GSK (formerly Novartis Vaccines and Diagnostics) fellowship from the
528 PhD program of the University of Siena, and AFH was a recipient of an Intra-European
529 Fellowship (PIEF-GA-2012-328377).

530

531 The authors declared the following interests: all authors, except MB and AFH, were
532 permanent employees of Novartis Vaccines at the time of the study. Following the acquisition
533 of Novartis Vaccines by the GSK group of companies in March 2015, all but MB and AFH are
534 now permanent employees of the GSK group of companies. FB, ID and GB report ownership
535 of GSK shares and/or restricted GSK shares.

536

537 Author Contributions

538 IS, GB, MB and AFH conceived and designed the experiments; MB, AFH and PD performed
539 the experiments; all authors analyzed the data, contributed to writing the manuscript,
540 reviewed and approved the final version.

541

REFERENCES

1. **Chambers HF, Deleo FR.** 2009. Waves of resistance: *Staphylococcus aureus* in the antibiotic era. Nat Rev Microbiol **7:**629-641.
2. **Olaniyi R, Pozzi C, Grimaldi L, Bagnoli F.** 2016. *Staphylococcus aureus*-Associated Skin and Soft Tissue Infections: Anatomical Localization, Epidemiology, Therapy and Potential Prophylaxis. Curr Top Microbiol Immunol doi:10.1007/82_2016_32.
3. **Tong SY, Davis JS, Eichenberger E, Holland TL, Fowler VG, Jr.** 2015. *Staphylococcus aureus* infections: epidemiology, pathophysiology, clinical manifestations, and management. Clin Microbiol Rev **28:**603-661.
4. **Pozzi C, Olaniyi R, Liljeroos L, Galgani I, Rappuoli R, Bagnoli F.** 2017. Vaccines for *Staphylococcus aureus* and Target Populations. Curr Top Microbiol Immunol doi:10.1007/82_2016_54.
5. **Cheng AG, DeDent AC, Schneewind O, Missiakas D.** 2011. A play in four acts: *Staphylococcus aureus* abscess formation. Trends Microbiol **19:**225-232.
6. **Centers for Diesease Control and Prevention.** 2013. Antibiotic resistance threats in the United States. http://www.cdc.gov/drugresistance/pdf/ar-threats-2013-508.pdf. Accessed 06/02/2017.
7. **Singh R, Ray P.** 2014. Quorum sensing-mediated regulation of staphylococcal virulence and antibiotic resistance. Future Microbiol **9:**669-681.
8. **Friedman DB, Stauff DL, Pishchany G, Whitwell CW, Torres VJ, Skaar EP.** 2006. *Staphylococcus aureus* redirects central metabolism to increase iron availability. PLoS Pathog **2:**e87.
9. **Somerville GA, Chaussee MS, Morgan CI, Fitzgerald JR, Dorward DW, Reitzer LJ, Musser JM.** 2002. *Staphylococcus aureus* aconitase inactivation unexpectedly inhibits post-exponential-phase growth and enhances stationary-phase survival. Infect Immun **70:**6373-6382.
10. **Torres VJ, Attia AS, Mason WJ, Hood MI, Corbin BD, Beasley FC, Anderson KL, Stauff DL, McDonald WH, Zimmerman LJ, Friedman DB, Heinrichs DE, Dunman PM, Skaar EP.** 2010. *Staphylococcus aureus* Fur regulates the expression of virulence factors that contribute to the pathogenesis of pneumonia. Infect Immun **78:**1618-1628.
11. **Cassat JE, Skaar EP.** 2012. Metal ion acquisition in *Staphylococcus aureus*: overcoming nutritional immunity. Semin Immunopathol **34:**215-235.
12. **Cassat JE, Skaar EP.** 2013. Iron in infection and immunity. Cell Host Microbe **13:**509-519.
13. **Sebulsky MT, Shilton BH, Speziali CD, Heinrichs DE.** 2003. The role of FhuD2 in iron(III)-hydroxamate transport in *Staphylococcus aureus*. Demonstration that FhuD2 binds iron(III)-hydroxamates but with minimal conformational change and implication of mutations on transport. J Biol Chem **278:**49890-49900.
14. **Sebulsky MT, Hohnstein D, Hunter MD, Heinrichs DE.** 2000. Identification and characterization of a membrane permease involved in iron-hydroxamate transport in *Staphylococcus aureus*. J Bacteriol **182:**4394-4400.
15. **Mariotti P, Malito E, Biancucci M, Lo Surdo P, Mishra RP, Nardi-Dei V, Savino S, Nissum M, Spraggon G, Grandi G, Bagnoli F, Bottomley MJ.** 2013. Structural and functional characterization of the *Staphylococcus aureus* virulence factor and vaccine candidate FhuD2. Biochem J **449:**683-693.

16. **Mishra RP, Mariotti P, Fiaschi L, Nosari S, Maccari S, Liberatori S, Fontana MR, Pezzicoli A, De Falco MG, Falugi F, Altindis E, Serruto D, Grandi G, Bagnoli F.** 2012. *Staphylococcus aureus* FhuD2 is involved in the early phase of staphylococcal dissemination and generates protective immunity in mice. J Infect Dis **206:**1041-1049.
17. **Sebulsky MT, Speziali CD, Shilton BH, Edgell DR, Heinrichs DE.** 2004. FhuD1, a ferric hydroxamate-binding lipoprotein in *Staphylococcus aureus*: a case of gene duplication and lateral transfer. J Biol Chem **279:**53152-53159.
18. **Sebulsky MT, Heinrichs DE.** 2001. Identification and characterization of *fhuD1* and *fhuD2*, two genes involved in iron-hydroxamate uptake in *Staphylococcus aureus*. J Bacteriol **183:**4994-5000.
19. **Horsburgh MJ, Ingham E, Foster SJ.** 2001. In *Staphylococcus aureus*, Fur is an interactive regulator with PerR, contributes to virulence, and Is necessary for oxidative stress resistance through positive regulation of catalase and iron homeostasis. J Bacteriol **183:**468-475.
20. **Bagnoli F, Fontana MR, Soldaini E, Mishra RP, Fiaschi L, Cartocci E, Nardi-Dei V, Ruggiero P, Nosari S, De Falco MG, Lofano G, Marchi S, Galletti B, Mariotti P, Bacconi M, Torre A, Maccari S, Scarselli M, Rinaudo CD, Inoshima N, Savino S, Mori E, Rossi-Paccani S, Baudner B, Pallaoro M, Swennen E, Petracca R, Brettoni C, Liberatori S, Norais N, Monaci E, Bubeck Wardenburg J, Schneewind O, O'Hagan DT, Valiante NM, Bensi G, Bertholet S, De Gregorio E, Rappuoli R, Grandi G.** 2015. Vaccine composition formulated with a novel TLR7-dependent adjuvant induces high and broad protection against *Staphylococcus aureus*. Proc Natl Acad Sci U S A **112:**3680-3685.
21. **Bacconi M, Haag AF, Torre A, Castagnetti A, Chiarot E, Delany I, Bensi G.** 2015. A stable luciferase reporter plasmid for in vivo imaging in murine models of *Staphylococcus aureus* infections. Appl Microbiol Biotechnol doi:10.1007/s00253-015-7229-2.
22. **Cheng AG, Kim HK, Burts ML, Krausz T, Schneewind O, Missiakas DM.** 2009. Genetic requirements for *Staphylococcus aureus* abscess formation and persistence in host tissues. FASEB J **23:**3393-3404.
23. **Becker KW, Skaar EP.** 2014. Metal limitation and toxicity at the interface between host and pathogen. FEMS Microbiol Rev **38:**1235-1249.
24. **Sheldon JR, Heinrichs DE.** 2015. Recent developments in understanding the iron acquisition strategies of gram positive pathogens. FEMS Microbiol Rev **39:**592-630.
25. **Hammer ND, Skaar EP.** 2011. Molecular mechanisms of *Staphylococcus aureus* iron acquisition. Annu Rev Microbiol **65:**129-147.
26. **Baba T, Bae T, Schneewind O, Takeuchi F, Hiramatsu K.** 2008. Genome sequence of *Staphylococcus aureus* strain Newman and comparative analysis of staphylococcal genomes: polymorphism and evolution of two major pathogenicity islands. J Bacteriol **190:**300-310.
27. **Berendt T, Byren I.** 2004. Bone and joint infection. Clin Med (Lond) **4:**510-518.
28. **Reniere ML, Skaar EP.** 2008. *Staphylococcus aureus* haem oxygenases are differentially regulated by iron and haem. Mol Microbiol **69:**1304-1315.
29. **Pishchany G, Dickey SE, Skaar EP.** 2009. Subcellular localization of the *Staphylococcus aureus* heme iron transport components IsdA and IsdB. Infect Immun **77:**2624-2634.

30. **Ventura CL, Higdon R, Kolker E, Skerrett SJ, Rubens CE.** 2008. Host airway proteins interact with *Staphylococcus aureus* during early pneumonia. Infect Immun **76:**888-898.
31. **Stites SW, Plautz MW, Bailey K, O'Brien-Ladner AR, Wesselius LJ.** 1999. Increased concentrations of iron and isoferritins in the lower respiratory tract of patients with stable cystic fibrosis. Am J Respir Crit Care Med **160:**796-801.
32. **Ghio AJ, Turi JL, Yang F, Garrick LM, Garrick MD.** 2006. Iron homeostasis in the lung. Biol Res **39:**67-77.
33. **Reid DW, Carroll V, O'May C, Champion A, Kirov SM.** 2007. Increased airway iron as a potential factor in the persistence of *Pseudomonas aeruginosa* infection in cystic fibrosis. Eur Respir J **30:**286-292.
34. **Corbin BD, Seeley EH, Raab A, Feldmann J, Miller MR, Torres VJ, Anderson KL, Dattilo BM, Dunman PM, Gerads R, Caprioli RM, Nacken W, Chazin WJ, Skaar EP.** 2008. Metal chelation and inhibition of bacterial growth in tissue abscesses. Science **319:**962-965.
35. **Ganz T.** 2007. Molecular control of iron transport. J Am Soc Nephrol **18:**394-400.
36. **Graham RM, Chua AC, Herbison CE, Olynyk JK, Trinder D.** 2007. Liver iron transport. World J Gastroenterol **13:**4725-4736.
37. **Pishchany G, McCoy AL, Torres VJ, Krause JC, Crowe JE, Jr., Fabry ME, Skaar EP.** 2010. Specificity for human hemoglobin enhances *Staphylococcus aureus* infection. Cell Host Microbe **8:**544-550.
38. **Endicott NP, Lee E, Wencewicz TA.** 2017. Structural Basis for Xenosiderophore Utilization by the Human Pathogen *Staphylococcus aureus*. ACS Infect Dis doi:10.1021/acsinfecdis.7b00036.
39. **Podkowa KJ, Briere LA, Heinrichs DE, Shilton BH.** 2014. Crystal and solution structure analysis of FhuD2 from *Staphylococcus aureus* in multiple unliganded conformations and bound to ferrioxamine-B. Biochemistry **53:**2017-2031.
40. **Jenkins A, Diep BA, Mai TT, Vo NH, Warrener P, Suzich J, Stover CK, Sellman BR.** 2015. Differential expression and roles of *Staphylococcus aureus* virulence determinants during colonization and disease. MBio **6:**e02272-02214.
41. **Chaves-Moreno D, Wos-Oxley ML, Jauregui R, Medina E, Oxley AP, Pieper DH.** 2016. Exploring the transcriptome of *Staphylococcus aureus* in its natural niche. Sci Rep **6:**33174.
42. **Szafranska AK, Oxley AP, Chaves-Moreno D, Horst SA, Rosslenbroich S, Peters G, Goldmann O, Rohde M, Sinha B, Pieper DH, Loffler B, Jauregui R, Wos-Oxley ML, Medina E.** 2014. High-resolution transcriptomic analysis of the adaptive response of *Staphylococcus aureus* during acute and chronic phases of osteomyelitis. MBio **5**.
43. **Tamura K, Stecher G, Peterson D, Filipski A, Kumar S.** 2013. MEGA6: Molecular Evolutionary Genetics Analysis version 6.0. Mol Biol Evol **30:**2725-2729.
44. **Letunic I, Bork P.** 2011. Interactive Tree Of Life v2: online annotation and display of phylogenetic trees made easy. Nucleic Acids Res **39:**W475-478.
45. **Monk IR, Shah IM, Xu M, Tan MW, Foster TJ.** 2012. Transforming the untransformable: application of direct transformation to manipulate genetically *Staphylococcus aureus* and *Staphylococcus epidermidis*. MBio **3**.
46. **Kreiswirth BN, Lofdahl S, Betley MJ, O'Reilly M, Schlievert PM, Bergdoll MS, Novick RP.** 1983. The toxic shock syndrome exotoxin structural gene is not detectably transmitted by a prophage. Nature **305:**709-712.

680 47. **Schneewind O, Mihaylova-Petkov D, Model P.** 1993. Cell wall sorting signals in
681 surface proteins of gram-positive bacteria. EMBO J **12:**4803-4811.

682

683

684 **FIGURE LEGENDS**

685 **FIG 1** Analysis of the intergenic region upstream of *fhuD2*. (A) Schematic of *fhuD1* and
686 *fhuD2* genomic context and promoter region within strain Newman. (B) Phylogenetic tree of
687 intergenic sequences upstream of *fhuD2,* extracted from 4135 *S. aureus* genomes. Seven
688 individual clusters representing sequence variants are colored. (C) Multiple sequence
689 alignment of representative sequence variants from each cluster. The start site of the coding
690 sequence is highlighted in blue, while predicted regulatory elements such as the Fur-binding
691 motif and -10 and -35 recognition sequences are highlighted in green and orange,
692 respectively.

693

694 **FIG 2** Fur-dependent iron regulation of *fhuD2***.** *S. aureus* Newman strain (NM) and its Fur
695 mutant (*Δfur)* harboring the *fhuD2* reporter plasmid were grown as 50 ml TSB cultures to
696 early/mid exponential phase and iron starvation was induced by adding dipyridyl to a final
697 concentration of 1 mM (DIP) or by adding an identical volume of the solvent (ethanol) to the
698 control culture (TSB). (A&B) Bioluminescence data were normalized using the CFUs of the
699 respective time points and are represented as expression levels relative to the wild-type TSB
700 culture prior to induction. (C&D) mRNA expression levels were determined for the
701 endogenous *fhuD2* gene and are represented as expression levels relative to the wild-type
702 TSB culture prior to induction. Data shown represent triplicate measurements from two
703 independent biological repeats. Statistical analysis was performed using ANOVA followed by
704 Tukey's post-test. ** $p<0.01$, ***$p<0.001$, **** $p<0.0001$, ns not significant.

705

706 **FIG 3** Visualization of *fhuD2* expression *in vivo*. CD1 mice were infected with strain
707 Newman carrying the *fhuD2* reporter plasmid and monitored daily by using the IVIS100®

imaging system. (A) Representative 2D pictures of the distribution of bioluminescent signals of mice acquired in a dorsal or ventral position at 2, 4 and 7 days post-intravenous challenge with the bioluminescent Newman strain. (B) Quantification of bioluminescence/mouse through ROI analysis. Values reported at day 0, are from non-infected mice.

FIG 4 Localization of bioluminescence by 3D and CT analysis of mice infected with *S. aureus* strain Newman carrying the *fhuD2* reporter plasmid. Images were collected 7 days post intravenous challenge. (A) Representative ventral 2D and (B) 3D reconstruction and (C-F) TAC analysis evidence that bioluminescence signals arise from bone, knee and kidneys sites and (G) representative dorsal 2D and (H) 3D reconstruction or (I) TAC analysis evidence bioluminescent signals in liver and in heart. Legend: K: kidney; B: bladder; H: heart; L: lung; Li: liver. For TAC analysis, we reported sagittal transversal sections.

FIG 5 Progression of *S. aureus* infection in various host organs. CD1 mice were infected with 10^7 CFU of *S. aureus* strain Newman. Organs (A, heart; B, Lungs; C, Livers and D, Kidneys) were collected at the defined time points, homogenized and CFU per ml of homogenized organ determined.

FIG 6 Quantification of *fhuD2* promoter activity in infected mouse organs. (A-D) Development of bioluminescence levels in the indicated organs throughout a 7-day infection time course. *fhuD2* promoter activity was determined as bioluminescence per CFU and fold changes were calculated as compared to the inoculum. (E-H) *fhuD2* mRNA levels: *fhuD2* promoter activity from the endogenous *fhuD2* gene was determined by qRT-PCR and fold changes were calculated relative to the inoculum before infection. Each symbol corresponds

732 to an organ of a single animal. Numbers depicted above the time points represent the mean
733 of the respective dataset. Statistical analysis was performed on logarithmic data using
734 ANOVA followed by Tukey's post-test and refers to the inoculum if not otherwise indicated.
735 *p<0.05, **p<0.01, ***p<0.001. Data plotted represent the mean of each group.
736
737

TABLES

Table 1 Strains and plasmids

Strains or plasmid	Relevant characteristics	Source or reference
***S. aureus* strains**		
Newman	MSSA, clumping factor overproducer, UK, CC8, CPS 5	(26)
RN4220	*hsdR*$^-$, restriction negative strain used for preparing plasmids	(46)
***E. coli* strains**		
DH5α	*supE*44 *lacU169* (w80lacZDM15) *hsdR*17 *recA*1 *endA*1 *gyrA*96 *thi*-1 *relA*1	Bethesda Research Laboratories
Plasmids		
pOS1	*S. aureus* ORI for Gram-positive strains; pBR322 plasmid replication in Gram-negative bacteria; Amp^R and Cm^R	(47)
pBluescript II SK (+)	Standard cloning vector, Amp^R	Stratagene
pIMAY	*E. coli*/*S. aureus* shuttle vector, temperature sensitive, Cm^R	(45)
pMABA-Par/TA-*lux*	pOS1 carrying *luxABCDE*, toxin/antitoxin (ε/ζ) + *par* system	(21)
pMABA-Par/TA-P$_{fhuD2}$-*lux*	pOS1 carrying *luxABCDE* under the control of the *fhuD2* promoter, toxin/antitoxin (ε/ζ) + *par* system	(21)"

Table 2 Primers

Primer name	Sequence (5'→3')	Application
Sa_16s_+332_F	GAGACACGGTCCAGACTCCT	qRT-PCR
Sa_16s_+437_R	ACGATCCGAAGACCTTCATC	"
Sa_*gyrB*_+238_F	ACGGATAACGGACGTGGTAT	"
Sa_*gyrB*_+339_R	GCCAAATTTACCACCAGCAT	"
Sa_*fhuD2*_+480_F	AGAAACAACTGCTAAAGACGGT	"
Sa_*fhuD2*_+594_R	ACCCCAGTTATCGCCGTAA	"
NWMN_1406_-796_XbaI_F	GGCCGCTCTAGACCTAAACTCATGCAACCTAGAC C	*fur* deletion
NWMN_1406_+6_BamHI_R	ACCATGGGATCCTTCCAACGATGTCCACTCC	"
NWMN_1406_+409_BamHI_F	TTGGAAGGATCCCATGGTGTGTGTGAAACGTG	"
NWMN_1406_+1197_KpnI_R	GAATTGGGTACCGTTTGCCTTTACACCATTTTG	"
NWMN_1406_-796_pIMAY_F	CGACTCACTATAGGGCGAATTGGAGCTCCCTAAA CTCATGCAACCTAGACC	"
NWMN_1406_+1197_pIMAY_R	CCTCACTAAAGGGAACAAAAGCTGGGTACCGTTT GCCTTTACACCATTTTG	"
NWMN_1406_-837_F	CAGCACAATCTATAATTTGTTCGGC	"
NWMN_1406_+1228_R	GTAACGTATGTGGCGTTAACGTC	"

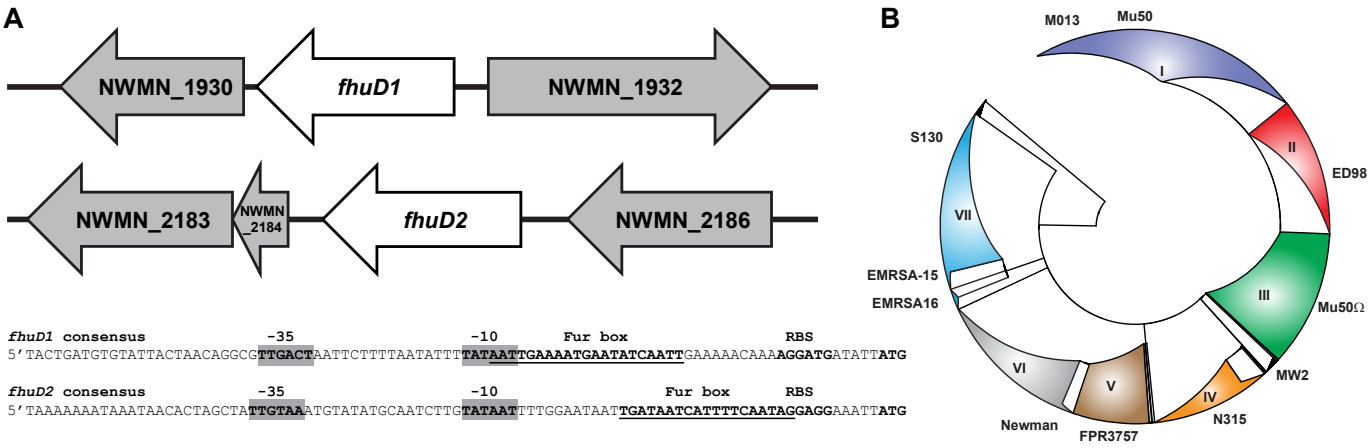

C

	-35	-10	Fur-box	Start
Newman	TAAAAAA-TAAATAACACTAGCTATTGTAAATGTATATGCAATCTTGTATAATTTTTGAATGATTGATAATCATTTTCAATAGGAGGAAATTATG			
FPR3757	TAAAAAA-TAAATAACACTAGCTATTGTAAATGTATATGCAATCTTGTATAATTTTTGAATGATTGATAATCATTTTCAATAGGAGGAAATTATG			
EMRSA-15	TAAAAAAATAAATAACACTAGCTATTGTAAATGTATATGCAATCTTGTATAATTTTGGAATGATTGATAATCATTTTCAATAGGAGGAAATTATG			
S130	TAAAAAAATAAATAACACTAGCTATTGTAAATGTATATGCAATCTTGTATAATTTTGGAATGATTGATAATCATTTTCAATAGGAGGAAATTATG			
EMRSA16	TAAAAAAATAAATAACACTAGCTATTGTAAATGTATATGCAATCTTGTATAATTTTGGAATAATTGATAATCATTTTCAATAGGAGGAAATTATG			
M013	TAAAAAA-TAAATAACACTAGCTATTGTAAATGTATATGCAATCTTGTATAATTTTGGAATAATTGATAATCATTTTCAATAGGAGGAAATTATG			
MW2	TAAAAAAATAAATAGCACTAGCTATTGTAAATGTATATGCAATCTTGTATAATTTTGGAATAATTGATAATCATTTTCAATAGGAGGAAATTATG			
ED98	TAAAAAAATAAATAGCACTAGCTATTGTAAATGTATATGCAATCTTGTATAATTTTGGAATAATTGATAATCATTTTCAATAGGAGGAAATTATG			
Mu50	TAAAAAAATAAATAGCACTAGCTATTGTAAATGTATATGCAATCTTGTATAATTTTGGAATAATTGATAATCATTTTCAATAGGAGGAAATTATG			
Mu50Ω	TAAAAAAATAAATAGCACTAGCTATTGTAAATGTATATGCAATCTTGTATAATTTTGGAATAATTGATAATCATTTTCAATAGGAGGAAATTATG			
N315	TAAAAAAATAAATAGCACTAGCTATTGTAAATGTATATGCAATCTTGTATAATTTTGGAATAATTGATAATCATTTTCAATAGGAGGAAATTATG			
Consensus	TAAAAAAATAAATAACACTAGCTATTGTAAATGTATATGCAATCTTGTATAATTTTGGAATAATTGATAATCATTTTCAATAGGAGGAAATTATG			

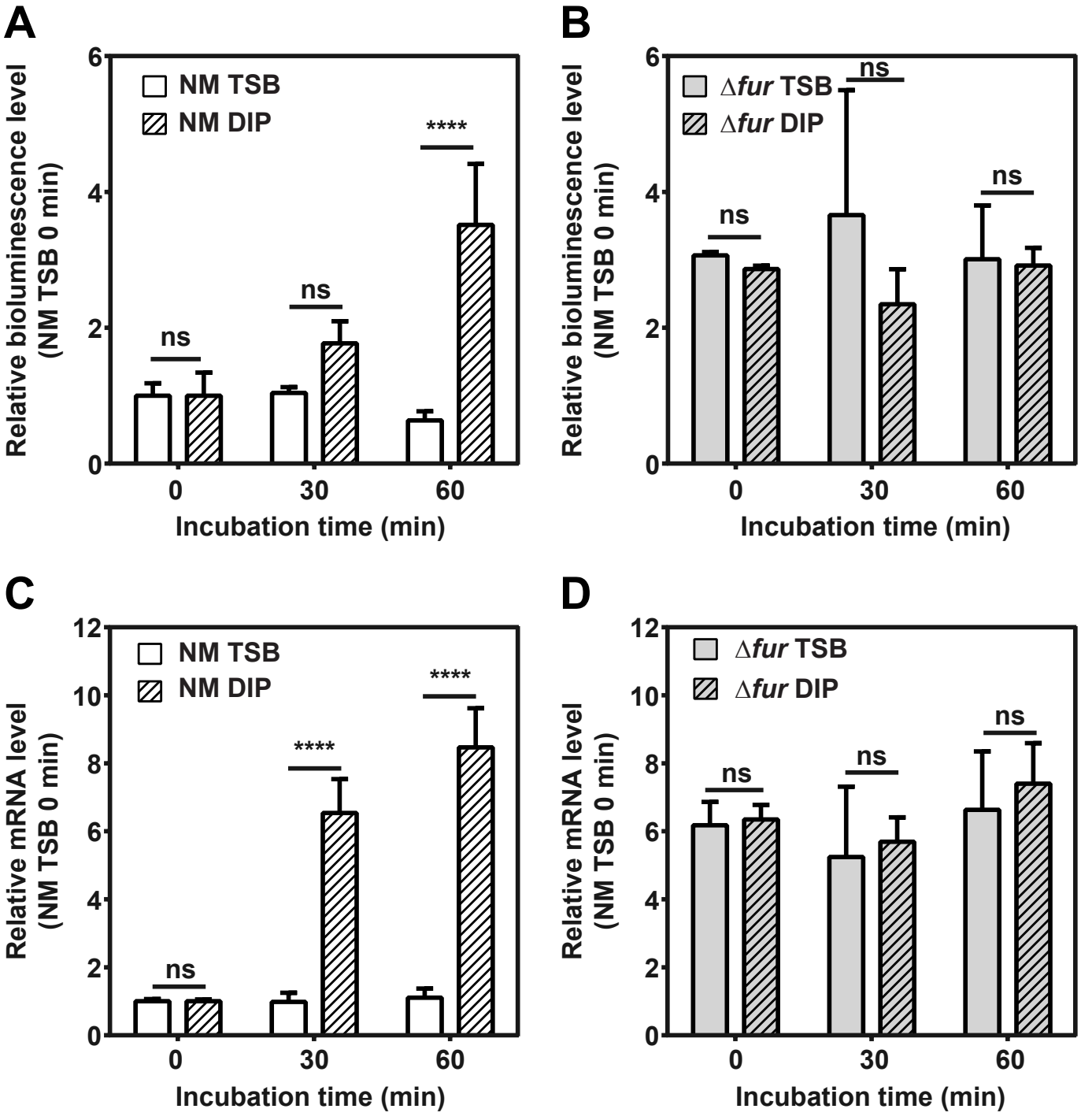

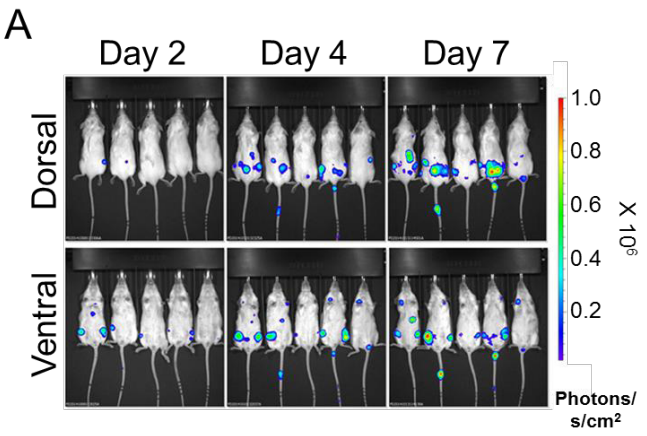

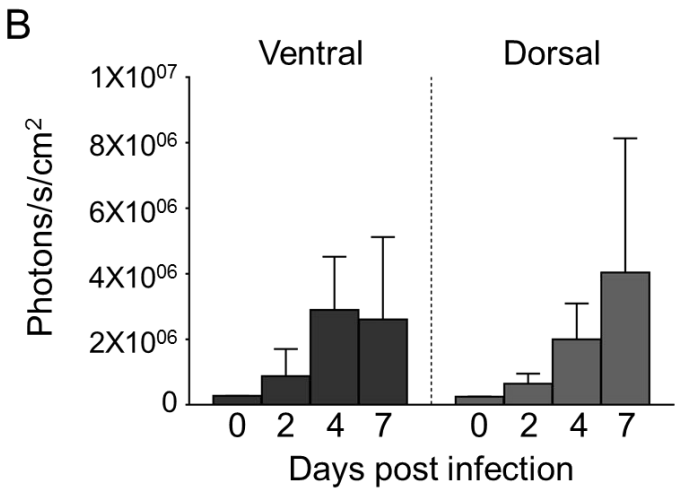

Infection and Immunity

IAI

Infection and Immunity